Title
Constraints on Inner Core Anisotropy Using Array Observations of P′P′

Journal
Geophysical Research Letters, 44(21)

ISSN
0094-8276

Authors
Frost, DA
Romanowicz, B

Publication Date
2017-11-16

DOI
10.1002/2017GL075049

Peer reviewed

Constraints on Inner Core anisotropy using array observations of P′P′

Authors: Daniel A. Frost[1]*, Barbara Romanowicz[1,2,3]

Affiliations:

[1]Earth & Planetary Science, University of California, Berkeley, California, USA

[2]Institut de Physique du Globe de Paris, Paris, France

[3]College de France, Paris, France

*Correspondence to: dafrost@berkeley.edu

Key points

- Detect inner core phase P′P′df (PKPPKPdf) at two high latitude seismic arrays
- Infer weak inner core anisotropy of 0.5-1.5% aligned with the rotation axis
- Observe stronger velocity anomalies with greater variability in magnitude in paths reflecting under the South Sandwich Islands

Abstract

Recent studies of PKPdf travel times suggest strong anisotropy (4% or more) in the quasi-western inner core hemisphere. However, the availability of paths sampling at low angles to the Earth's rotation axis (the fast axis) is limited. To augment this sampling, we collected a travel time dataset for the phase P′P′df (PKPPKPdf), for which at least one inner core leg is quasi-polar, at two high latitude seismic arrays. We find that the inferred anisotropy is weak (on the order of 0.5 to 1.5%), confirming previous results based on a much smaller P′P′ dataset. While previous models of inner core anisotropy required very strong alignment of anisotropic iron grains, our results are more easily explained by current dynamic models of inner core growth. We observe large travel time anomalies when one leg of P′P′df is along the South Sandwich to Alaska path; consistent with PKPdf observations, and warranting further investigation.

1. Introduction

Inner core anisotropy with the fast axis aligned with the Earth's rotation axis was proposed thirty years ago based on observations of seismic body waves traveling faster along paths close to the Earth's rotation axis than those traveling equatorially (Morelli et al., 1986) and on anomalous splitting of core-sensitive normal modes (Woodhouse et al., 1986). Continued investigation has refined measurements of the velocity structure of the inner core, revealing increasing complexity (for review see Deuss, 2014; Tkalcic, 2015). In the most recent models, the inner core consists of two roughly equal hemispheres with different levels of P-velocity anisotropy: up to 4.8% in the quasi-western hemisphere, and up to 1.4% in the quasi-eastern hemisphere (Tanaka and Hamaguchi, 1997; Irving and Deuss, 2011). The location and depth extent of the boundaries is not well constrained (Lythgoe et al., 2014; Irving, 2016). Depth dependence of the anisotropy has been proposed, along with evidence for a distinct Innermost Inner Core (IMIC) of 300-600 km in radius, with anisotropy inclined to the rotation axis (Ishii and Dziewonski, 2002; Beghein and Trampert, 2003; Cao and Romanowicz, 2007; Sun and Song, 2008; Wang et al., 2015).

The seismically inferred anisotropy motivates studies of inner core mineral texture and composition. The proportion and nature of any light element in the inner core affects bulk properties (e.g. Nguyen and Holmes, 2004), while crystal structure and alignment impacts anisotropy (e.g. Wenk et al., 2000). The growth behavior of the inner core may have influenced the development of anisotropy (Monnereau et al., 2010, Lincot et al., 2015). Accurate understanding of the distribution of velocities in the inner core will inform its formation and deformation history.

Absolute PKPdf residual travel times with respect to 1D isotropic reference models are sensitive to errors in source parameters and to uncorrected mantle heterogeneity. To minimize these effects, they are often referred to a core phase that does not interact with the inner core, such as PKPab

or PKPbc. Unfortunately; there are few PKPdf measurements for paths close to the rotation axis, due to the global distribution of earthquakes and stations. Furthermore, many of these paths correspond to sources in the South Sandwich Islands (SSI) observed in Alaska and Siberia. These particular paths show large variability in PKPdf travel time anomalies (Romanowicz et al., 2003; Tkalcic, 2010; Romanowicz and Wenk 2017). While large residuals are observed on some polar paths (implying up to 8.8% velocity anisotropy e.g. Lythgoe et al., 2014), owing to the limited sampling, these measurements may not be representative of the whole inner core. Further, independent travel time measurements of inner core sensitive phases are necessary to constrain the magnitude and spatial extent of anisotropy.

The phase P′P′df is the underside surface reflection of the PKPdf wave, and it traverses the inner core twice (Fig. 1a). It allows different sampling of the inner core than is available in PKPdf studies (Fig. 1b and 1c). Following Bréger et al. (2000) and Rost and Garnero (2004), we measured P′P′df residual times along previously unsampled paths, spanning a range of angles (ξ) made by the path in the inner core with the rotation axis. Previous studies of the inner core using these phases did not find evidence of strong anisotropy.

2. Methods

We collected data from 256 M>6 events, that occurred within 0-to-65° epicentral distance of two high-latitude IMS arrays, Eilson (IL) in Alaska and Yellowknife (YK) in Canada from 1995 to 2012 (Supplementary Table 1). Origin times and event locations are taken from the Reviewed Event Bulletin (REB). The two P′P′df legs pass through the inner core at different angles to the rotation axis. In our dataset many paths have one inner core leg inclined within 35° of the rotation axis (often the receiver-side leg) and a second leg oriented equatorially (Supplementary Figure 1). Most paths in our dataset (60%) turn in a limited depth range between 5321-5621 km. Deeper paths do not cover a sufficient range of ξ angles for us to resolve depth dependence of anisotropy.

P′P′df is a low amplitude phase, having twice travelled through the strongly attenuating inner core (e.g. Li and Cormier, 2002), thus we stack traces to amplify the phase relative to the noise. We filter data between 0.4 and 1.5 Hz, select a time window around the predicted arrivals of P′P′df, P′P′bc, and P′P′ab, and beam traces on slownesses from 0 to 8 s/deg, and back-azimuths from -180 to 180° (relative to the great-circle path) (Davies et al., 1971). From the linear beams we calculate F-vespagrams by applying the F-statistic, a coherence measure that is effective at suppressing aliasing, thus sharpening the slowness and back-azimuth resolution at an array (Equation 1. Blandford, 1974; Selby, 2008). The coherence, F, is computed from the ratio of the sum of the energy in the beam, b, to the summed differences between the beam and each trace used to form the beam, x_i, in a time window, M, normalised by the number of traces in the beam, N.

$$F = \frac{N-1}{N} \frac{\sum_{t=1}^{M} b(t)^2}{\sum_{t=1}^{M} \sum_{i=1}^{N} (x_i(t) - b(t))^2}$$

Equation 1

Using both slowness-time and backazimuth-time F-vespagrams, individual beams and F-traces (Fig. 2. See Supplementary Figures 2-6 for vespagrams of other qualities), we handpick the onsets of P′P′df, P′P′ab, and P′P′bc, where present, measured relative to predictions from model ak135 (Kennett et al., 1995), corrected for ellipticity (Kennett and Gudmundsson, 1996). We visually assess waveform similarities between phases to aid identification. The P′P′ab waveform is Hilbert transformed for comparison with the P′P′df waveform. Slowness and back-azimuth are used to aid picking of the specular reflections and to help with discounting contamination from other events or phases. We only select signals arriving within ~30° of the great-circle path at slownesses within 1s/deg of those predicted by ak135. We use a similar method of F-vespagrams and beams to measure the direct P-wave travel time anomaly for each event relative to ak135, corrected for ellipticity.

Where present, phases are picked as poor or good, dependent on the above characteristics. We discard 141 events, leaving 115 well-picked events (57 at IL and 58 at YK), each with at least a P′P′df phase, and possibly a P′P′bc and a P′P′ab. Average picking accuracy is ~0.2 s. We calculate P′P′ab-df and P′P′bc-df differential residual times, and P′P′df absolute residual times, where positive and negative residual and absolute times, respectively, indicate a fast inner core, thus we reverse the sign of P′P′df absolute measurements for comparison with the differential measurements. We apply corrections calculated for the direct P-wave to account for event mislocation and near-surface structure. For each event, we calculate the signal-to-noise ratio of P′P′df relative to noise in a 10 s long window starting 50 s prior to the predicted arrival of P′P′df.

Differential measurements of P′P′ab-df and P′P′bc-df are used to reduce the influence of unmodeled mantle and source effects. Still, it may be necessary to apply corrections for mantle and crustal structure before attributing the residuals to the inner core (e.g. Bréger et al., 1999). Given the long path of P′P′ab in the lower mantle and its large separation from the P′P′df path, P′P′ab-df residual measurements are less reliable than P′P′bc-df measurements, however P′P′bc exists only for a small range of source-receiver distances (between major arc distances of 290-311°). At these distances, the direct waves, P′P′ab, P′P′bc, and P′P′df arrive within a short time window, making phase identification difficult. For events at larger source-receiver distances there is greater time separation between phases, thus we use P′P′df absolute residuals and P′P′ab-df differential residuals to increase our coverage.

3. Results

We observe up to three direct arrivals in the P′P′ time window, and other additional arrivals and noise, discussed in section 4.1.

The measured residual arrival times show large scatter, but are, on average, low (mean and standard deviation: P′P′ab-df = 1.04±2.72 s, P′P′bc-df = 1.02±2.09 s, and P′P′df = -3.14±2.64 s for data with SNR>2, Fig. 3) compared with up to 10 s predicted by some anisotropy models. These low values are consistent for data with lower signal-to-noise ratios (Supplementary Fig. 7). Residual travel time anomalies show spatial variability. In particular, paths reflecting under the source region of the SSI events show rapid changes in anomalies with small changes in path (Fig. 3).

We convert travel time anomalies to velocity anomalies relative to ak135 as: $\frac{dT}{T} = \frac{-dV}{V}$, where T and V are a reference travel-time and velocity in the inner core, respectively, to account for differences in inner core path lengths. We attribute the entire travel time anomaly to the inner core. We are unable to separate the influence of the two, differently oriented, paths through the inner core, hence we consider the residual time as a single cumulative anomaly and characterize the whole P′P′df path by the average of the two angles (ξ_1 and ξ_2) made with the rotation axis. Scatter in the measurements is reduced (mean and standard deviation: P′P′ab-df = 0.49±0.21 s, P′P′bc-df = 0.43±0.26 s, and P′P′df = 0.48±0.26 s for data with SNR>2, Fig. 3). We find a weak trend of increasing velocity anomalies with decreasing average ξ angle (Fig. 4), consistent with the results of past P′P′df studies (Bréger et al., 2000; Rost and Garnero, 2004).

4. Discussion

Our P′P′df travel time measurements suggest weak anisotropy in the inner core. Here, we discuss the reliability of the measurements, possible sources of contamination, the magnitude of the anisotropy relative to previous studies, and the implications for core structure.

4.1 Robustness of observations

P′P′ is a maximum travel time phase, such that scattering or reflection from dipping reflectors in the crust at locations other than the specular reflection point will produce precursors to the main phase. However, these precursory waves arrive from different directions than the main phase (Supplementary Figure 8). Therefore, we pick waves that arrive with slowness and back-azimuth most consistent with the predictions for the main P′P′ waves. We observe slowness and back-azimuths departures from 1D model predictions, which, on average at YK are: P′P′df 0.7 s/deg±1.0 and 22.5 ° ±15.5, P′P′bc 0.5 s/deg±0.2 and 18.2 ° ±13.8, and P′P′ab 1.1 s/deg ±1.2 and 11.4 ° ±9.2, and at IL: P′P′df 0.6 s/deg±0.5 and 65.3°±33.8, P′P′bc 0.4 s/deg±0.3 and 38.9°±26.1, and P′P′ab 1.5 s/deg±1.0 and 57.8°±40.4. Furthermore, we find that the slowness of P′P′ab is more sensitive to small changes in lower mantle velocities than P′P′df or P′P′bc.

We perform resolution tests to determine the ability of the arrays to correctly determine slowness and back-azimuth for P′P′. We use a synthetic wavelet of a similar duration to our data, combined with real noise from each array, scaled to have SNR of

2, and filter the data between 0.4 and 1.5 Hz. We find that back-azimuth resolution strongly depends upon incoming slowness (Supplementary Table 2). For slownesses typical of P′P′df (~0.5 to 1.5 s/deg), we expect to resolve the signal to within, on average, 1.0 s/deg slowness and ~65° back-azimuth for IL, and 0.2 s/deg slowness and 10° back-azimuth for YK. Thus, especially for the lower slowness signals at IL, large azimuthal anomalies are expected. Disparities in resolution limits between the arrays result from differences in the width (aperture) of the array and the distribution of stations.

4.2 Possible contamination by mantle structure

The variability in travel time residuals may result from heterogeneity on other parts of the path. While differential measurements and P wave corrections should account for crust and upper mantle structure and source mislocations, the influence of lower mantle structure may remain. In addition, strong anomalies resulting from subducted slabs could cause significant travel time anomalies between the two paths in a differential phase pair (Weber, 1990; Helffrich and Sacks, 1994). Laterally varying upper mantle structure could contribute to the scatter that we observe here, but it is unlikely to be the sole cause of the positive velocity anomaly.

To evaluate the influence of not-accounted-for mantle structure, we calculate corrections for the P′P′ phases from several global tomographic models by 1D ray tracing through the model and calculating the anomaly accumulated along the path. We use P-wave models GAP_P4 (Obayashi et al., 2013) and MIT_P08 (Li et al., 2008) and S-wave models S40RTS (Ritsema et al., 2011) and SEMUCB-WM1 (French and Romanowicz, 2014). The S-wave models are scaled to P-wave velocities using a constant factor of 0.5 for SEMUCB-WM1 and, for S40RTS, a factor linearly decreasing from 0.8 at the surface to 0.33 at the CMB (Ritsema and van Heijst, 2002). Differential mantle corrections are, on average, small at around 0.2 s for P′P′ab-df and P′P′bc-df, and 0.3 to 0.7 s for P′P′df. Nonetheless, the corrections often reduce the spread of outliers implying that some of the scatter does result from mantle structure (Supplementary Figures 9 and 10). However, tomographic methods only resolve the broader scales of mantle heterogeneity (100s to 1000s km), thus the true corrections for mantle structure may be larger.

Strongly anomalous and laterally discontinuous, small-scale lower mantle structures, such as Ultra-Low Velocity Zones (ULVZs) and the D′′ layer, may cause sharp changes in differential travel times between closely located paths (Bréger et al., 2000), potentially influencing one phase of a P′P′ pair while leaving the travel time of the other unperturbed. To generate the observed positive residual times a ULVZ would have to delay the P′P′ab or P′P′bc phase or the region outside of the ULVZ would need to advance the P′P′df wave. For parameters typical of ULVZs (Garnero and Helmberger, 1998; Rost et al., 2006) and fast regions in D′′ (Weber and Körnig,

1992), even for the longest possible P′P′ab and P′P′df paths with the greatest possible separation and the most time spent in the lower mantle, these structures would produce travel time anomalies of around 1.5 s and 0.6 s, respectively. Multiple interactions with ULVZs or fast regions of D" could produce significant travel time anomalies, but this is unlikely. Thus while localized mantle structure may explain some of the observed scatter, it would be insufficient to explain all of the differential travel time residuals.

Topography on either the CMB or Inner Core Boundary (ICB) could cause differential travel-time anomalies, depending on ray piercing location. Scales of CMB topography are not well known, but are estimated to be less than 2 km in height (e.g. Soldati et al., 2011) which would produce a maximum of 0.01s for P′P′ab-df and less so for P′P′bc-df. Meanwhile, the maximum estimate ICB topography of 5 km amplitude over 10 km vertical scale (Cao et al., 2007) would produce a 0.04 s anomaly. While four boundary crossings of P′P′ would multiply these anomalies, the total would still be below the pick resolution, thus likely undetectable.

4.3 Strength of anisotropy

We compare the inferred P′P′ anisotropy to several inner core anisotropy models constructed from PKP (Irving and Deuss, 2011). Using the PKP models, we predict the overall velocity anomaly each P′P′ path would experience by combining the velocity anomaly along each inner core leg according to its ξ angle. We make predictions for uniform anisotropy models and hemispherical anisotropy models where each P′ leg experiences one of two anisotropic structures depending on the location of the P′ path mid point, according to hemisphere boundaries derived from Irving and Deuss (2011). The hemispherical PKP model is less anisotropic in the eastern (0.5%) than in the western (4.8%) hemisphere. While previous studies have found hemispherical isotropic velocity anomalies in the upper inner core (Waszek et al., 2011), with the exception of two paths, our P′P′ data sample both fast and slow isotropic hemispheres, thus the effect of this layer would cancel out.

We find large scatter in the absolute P′P′df residuals, thus we compare data with and without them to the PKP anisotropy models. Without the P′P′df data our observations most closely match predictions from the uniform model with 1.4% anisotropy, which is much weaker than most PKPdf models (Fig. 4). An exception to this is the small range of ξ angles dominated by paths reflecting under the SSI, where observed velocity anomalies are, on average, larger than those at both greater and smaller ξ angles. When events reflecting under the SSI are removed, the remaining observations even better match the 1.4% anisotropy model (Supplementary Figure 11). When the P′P′df data is included and a moving average is calculated to reduce the influence of outliers, our data show slightly stronger anisotropy of 1.5-2% (Supplementary Figure 12). Both with and without P′P′df data, our observations are significantly weaker than the PKP model

constructed using both eastern and western hemisphere anisotropy models from Irving and Deuss (2011).

The P′P′ differential travel times represent the cumulative effect of inner core structure, thus we are unable to determine where along either of the two inner core paths the travel time anomaly is acquired. We construct a range of synthetic inner core anisotropy models by scaling an existing one. We grid search for the strength of anisotropy on the east and west hemispheres that minimizes the RMS misfit between the synthetic velocity anomaly (of both hemispheres combined) and the observed velocity anomaly for all data at all ξ angles (Supplementary Figure 13). The best fitting anisotropy strongly depends on the data used and minima are poorly constrained. When absolute P′P′df observations are included, the data is best fit by a model with ~1% anisotropy in the western hemisphere and close to no anisotropy in the eastern hemisphere. Meanwhile, when only P′P′ab-df and P′P′bc-df observations are used, the data is best fit by either 1% anisotropy in the eastern hemisphere and no anisotropy in the western hemisphere, or roughly uniform anisotropy of ~0.5%. When data from paths reflecting under the South Sandwich Islands are included the best fitting model shows stronger anisotropy in the western hemisphere. While this suggests some interesting trends, we are reluctant to interpret them given the non-unique results.

4.4 Testing of model robustness

We construct a new model of cylindrical inner core anisotropy as a perturbation to a spherically symmetric model, parameterized as (Creager, 1992):

$$\frac{\delta v}{v} = a + b\,cos^2\,\xi + c\,cos^4\xi$$

Equation 2.

where v and δv represent the reference velocity and velocity perturbations, respectively. The coefficient a represents the difference between the apparent equatorial velocity and the reference model, b and c describe the variation of anisotropic velocity as a function of ξ, and the maximum amplitude of the anisotropy is thus $b + c$. We fit a curve to the data using an L1-norm to account for outliers. As we have no constraints beyond $\xi = 50°$, the model is required to reach 0% anisotropy at $\xi = 90°$.

We test the robustness of this model by bootstrapping the dataset. We calculate the mean and standard deviation across 1000 bootstrapped models and derive coefficients a, b, and c for this model. We construct one isotropic model (b=c=0) to test the misfit reduction. Applying mantle corrections to the residual times and recalculating the anisotropy model results in negligible improvements of the fit for all tomographic models (Supplementary Figure 14). Coefficients and RMS misfit for all models are given in Supplementary Table 3. We find anisotropy of ~0.5%, weaker than observed in the moving averages (Fig. 4b), as the curve tries to account for the observation of a lower

velocity anomaly (0.4%) closer to the rotation axis (~15°) rather than anomalies further away from it. The standard deviation of the bootstrapped models, which includes models where this data point has been removed, ranges from 0 to 1% anisotropy.

4.5 Implications for core structure

Paths reflecting under the SSI show larger velocity anomalies and greater scatter than other paths at lower ξ. This supports previous observations of variability in PKPdf velocity anomalies on similar paths (Romanowicz et al., 2003; Tkalcic, 2010; Romanowicz and Wenk, 2017). The cause of this variability may be in the inner or outer cores, or within the mantle. Possibly, the structure of the subducting slab in the South Sandwich Islands may influence differential travel times and might not be suitably represented in global tomographic models.

The anisotropic velocity structure of the inner core relates to its composition, physical state, and dynamics. Experiments and first-principles calculations show uncertainty over whether the inner core comprises hexagonally close-packed (hcp) or body-centered cubic (bcc) iron (Mikhaylushkin et al., 2007; Modak et al., 2007; Belonoshko et al., 2008; Tateno et al., 2010). While the anisotropy of a single crystal depends on its phase, the effective anisotropy of the bulk core will also depend on the degree of alignment of the crystals. Dynamic models of core growth have suggested that cubic phases of iron (bcc and face-centered cubic) could produce global anisotropy up to 1% seismic anisotropy but more likely ~0.5% (Lincot et al., 2015), while hcp iron could produce 1-3% anisotropy (Lincot et al., 2016), depending on the dominant slip system of plastic deformation and method of core growth. Other methods suggest global anisotropy would be similar for a core comprising hcp or a bcc fiber structure (Romanowicz, et al., 2015). Our observations imply that either crystal structure is possible, but that the inner core may not need be as strongly anisotropic as previously thought. The lateral variability in observed travel times suggests either an inner core comprising multiple domains (Tkalcic, 2010), potentially generated by variability in the degree of crystal alignment (Lincot et al., 2015), or heterogeneity within or outside of the inner core.

5. Conclusion

We have assembled a dataset of travel time anomalies for P′P′ waves travelling through the inner core at previously unsampled locations. Our observations indicate at most 0.5-1.5% anisotropy aligned with the Earth's rotation axis, confirming the results of Bréger et al. (2000) and Rost and Garnero (2004). Anisotropy in the inner core may not be as strong as suggested in some recent studies. However, for paths with P'P' surface reflections located near the SSI, residual travel times show large variability, consistent with PKPdf observations. This suggests anomalous local structure within the inner core, in the upper mantle under the SSI or any part of the mantle and core sampled by these paths.

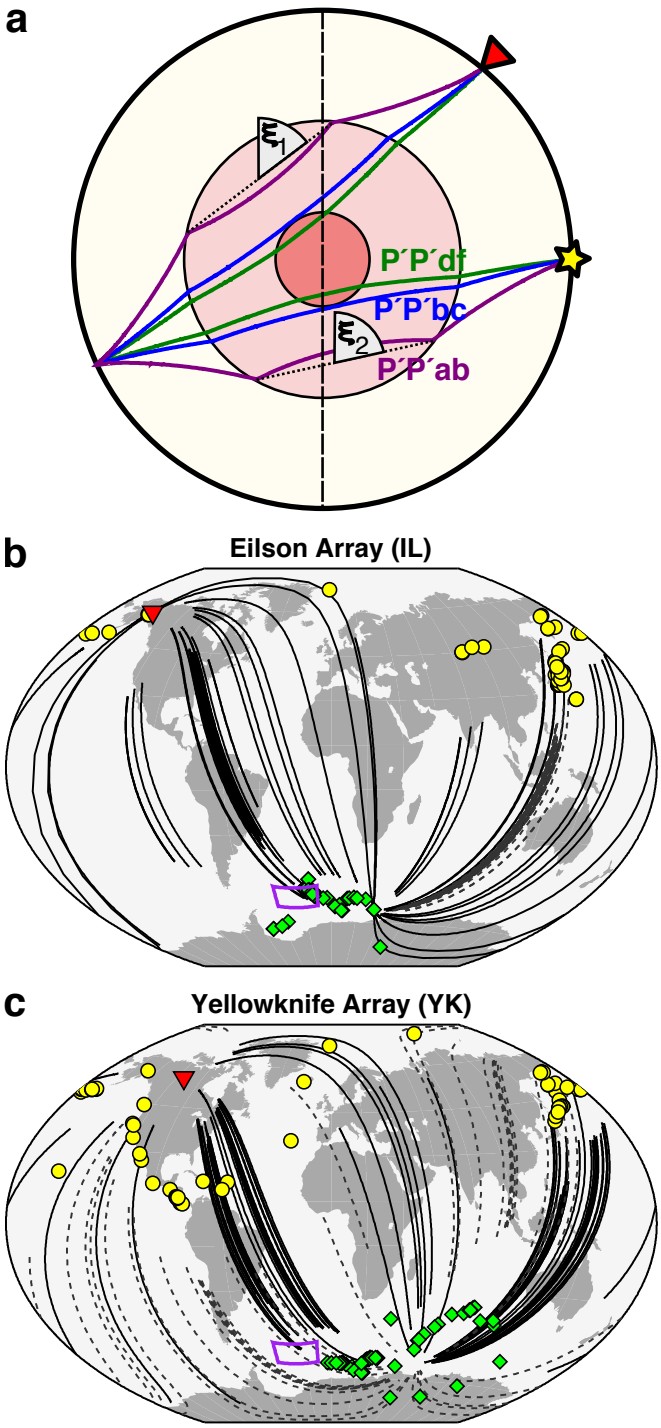

Figure 1. (a) Phases of P′P′ (also written PKPPKP). Angles of the inner core paths relative to the rotation axis (dashed line) are represented by ξ_1 and ξ_2 for source and receiver-side paths, respectively. Distribution of inner core paths between sources (circles), surface reflection points (diamonds), and arrays (triangles) for events to (b) Eilson and (c) Yellowknife arrays. Polar ($\xi \leq 35°$) and equatorial ($\xi > 35°$) paths are

drawn as solid and dashed lines, respectively. The box describes the source region of South Sandwich Island earthquakes.

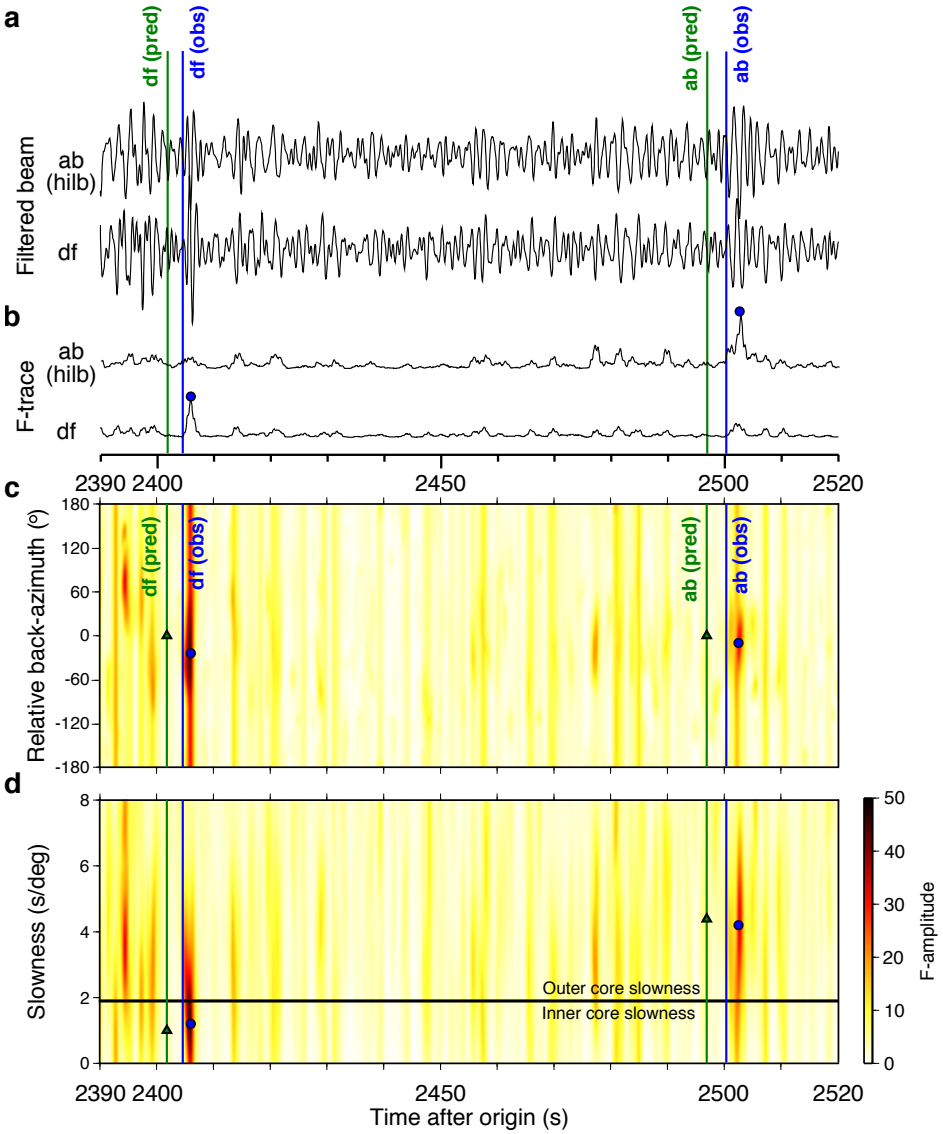

Figure 2. Beams and array processing of a M6.5 event which occurred on 15/08/2007 in the Aleutian Islands at a depth of 9 km, recorded at YK. (a) Beams and F-traces formed on P′P′ab and P′P′df slownesses and back-azimuths. F-vespagrams formed for a range of (b) back-azimuths and (c) slownesses. Predicted times and slownesses from ak135 are shown by green triangles and lines. Observations are marked by blue lines representing onset times and circles showing the maximum F-amplitude, accounting for the time separation between the picks and peaks.

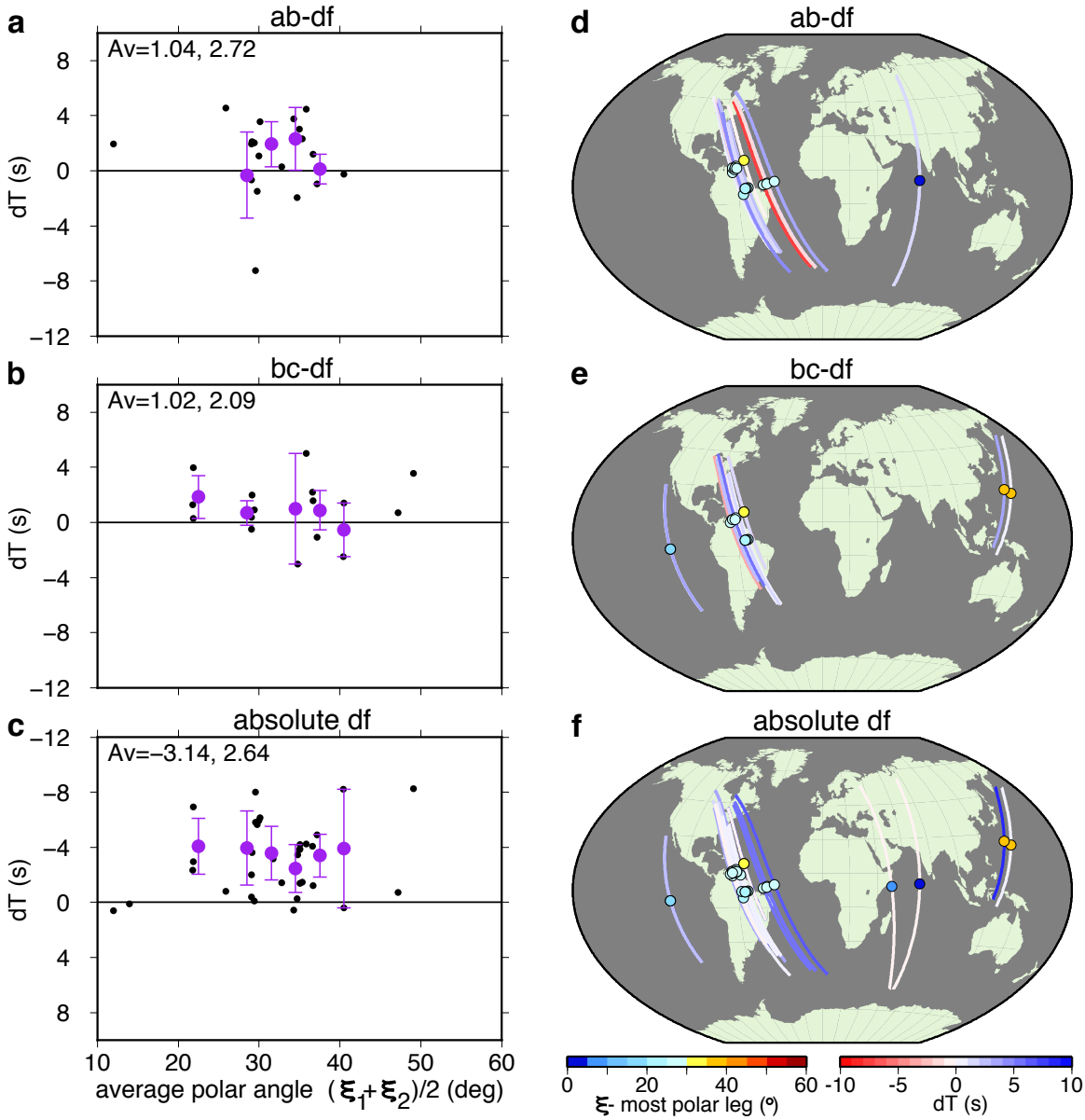

Figure 3. Residual travel times as a function of average angle to the rotation axis for (a) P′P′ab-df and, (b) P′P′bc-df differential measurements, and (c) P′P′df absolute measurements. Individual measurements are shown by points, while moving averages (in 3° bins with no overlap, for bins containing a minimum of 2 observations) are shown by purple circles with one standard deviation error bars. Residual travel times (line color) plotted along the inner core path, for only the most polar of the source- and receiver-side paths (ξ shown by circle color), for (d) P′P′ab-df differential measurements, (e) P′P′bc-df differential measurements, and (f) P′P′df absolute measurements. Data have SNR>2, for data at lower SNR values see Supplementary Figure 7.

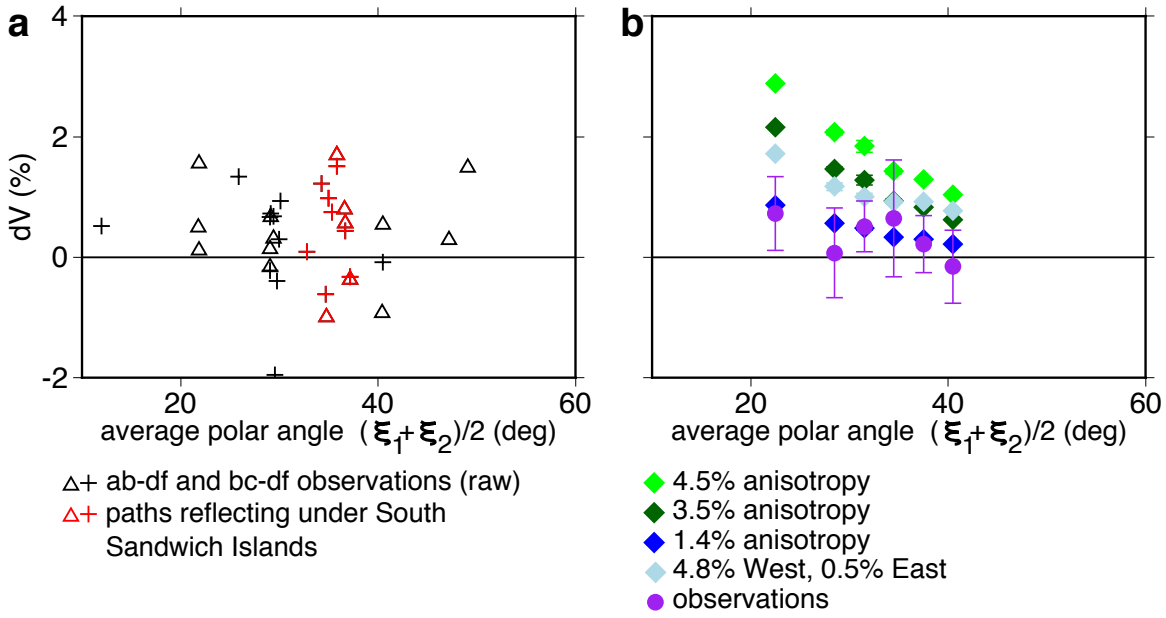

Figure 4. Observed velocity anomalies from P′P′ab-df and P′P′bc-df differential residual travel times, as a function of average angle to the rotation axis. (a) Raw measurements for all observations displayed as crosses and triangles for P′P′ab-df and P′P′bc-df, respectively (SNR>2). Velocity anomalies for paths reflecting under the South Sandwich Islands source region are shown in red. (b) Moving averages (calculated as in Fig. 3) of observed velocity anomalies (purple circles) with one standard deviation error bars, and predicted velocity anomalies calculated from several anisotropy models for the observed events (diamonds).

Acknowledgements

We thank the Prototype International Data Centre (pIDC) for development and distribution of the REB and the CTBTO for access to the waveform data from the IMS arrays. Waveform data for the Yellowknife and Eilson arrays are available from the Canadian National Data Centre at http://www.earthquakescanada.nrcan.gc.ca/stndon/AutoDRM/autodrm_req-en.phpcndc and the Incorporated Research Institutions for Seismology at http://ds.iris.edu/ds/nodes/dmc/forms/breqfast-request/, respectively. Our measurements are presented in Supplementary Table 4. This work was supported by NSF grants EAR-1135452 and EAR-1417229.

References

Beghein, C. & Trampert, J., 2003. Robust normal mode constraints on inner-core anisotropy from model space search, Science, 299, 552–555.

Belonoshko, A., Skorodumova, N. V., Rosengren, A., & Johansson, B., 2008. Elastic Anisotropy of Earth's Inner Core, Science, 319, 797–800.

Blandford, R. R., 1974. An automatic event detector at the Tonto Forest seismic observatory, Geophysics, 39, 633–643.

Bréger, L., Romanowicz, B., & Tkalcic, H., 1999. PKP(BC-DF) travel time residuals and short scale heterogeneity in the deep earth, Geophys. Res. Lett., 26(20), 3169–3172.

Bréger, L., Romanowicz, B. A., & Rousset, S., 2000. New constraints on the structure of the inner core from P'P', Geophys. J. Int., 27(17), 2781–2784.

Bréger, L., Tkalcic, H., & Romanowicz, B. A., 2000. The effect of D" on PKP (AB-DF) travel time residuals and possible implications for inner core structure, Earth Planet. Sci. Lett., 175, 133–143.

Cao, A., Masson, Y., & Romanowicz, B., 2007. Short wavelength topography on the inner-core boundary, Proc. Nat. Acad. Sci. USA, 104, 31–35.

Cao, A. & Romanowicz, B., 2007. Test of the innermost inner core models using broadband PKIKP travel time residuals, Geophys. Res. Lett., 34, 1-5

Creager, K. C., 1992. Anisotropy of the inner core from differential travel times of the phases PKP and PKIKP, Nature, 356.

Davies, D., Kelly, E. J., & Filson, J. R., 1971. Vespa Process for Analysis of Seismic Signals, Nat. Phys. Sci., 232, 8–13.

Deuss, A. F., 2014. Heterogeneity and Anisotropy of Earth's Inner Core, Ann. Rev. Earth planet. Sci., 42, 103–126.

French, S. W. & Romanowicz, B. A., 2014. Whole-mantle radially anisotropic shear velocity structure from spectral-element waveform tomography, Geophys. J. Int., 199, 1303–1327.

Garnero, E. J. & Helmberger, D. V., 1998. Further structural constraints and uncertainties of a thin laterally varying ultralow-velocity layer at the base of the mantle, J. Geophys. Res., 103, 12495–12509.

Helffrich, G. & Sacks, S., 1994. Scatter and bias in differential PKP travel times and implications for mantle and core phenomena, Geophys. Res. Lett., 21, 2167-2170.

International Seismological Centre, On-line Bulletin, http://www.isc.ac.uk, Internatl. Seismol. Cent., Thatcham, United Kingdom, 2014.

Irving, J. C. E., 2016. Imaging the inner core under Africa and Europe, Phys. Earth planet. Int., 254, 12–24.

Irving, J. C. E. & Deuss, A., 2011. Hemispherical structure in inner core velocity anisotropy, J. Geophys. Res., 116, 1–17.

Ishii, M. & Dziewonski, A. M., 2002. The innermost inner core of the earth: Evidence for a change in anisotropic behavior at the radius of about 300 km, Proc. Nat. Acad. Sci. USA, 99, 14026–14030.

Kennett, B. L. N. & Gudmundsson, O., 1996. Ellipticity corrections for seismic phases Ellipticity corrections for seismic phases, Geophys. J. Int., 127, 40–48.

Kennett, B. L. N., Engdah, E. R., & Buland, R., 1995. Constraints on seismic velocities in the Earth from traveltimes, Geophys. J. Int., 122, 108–124.

Li, C., van der Hilst, R. D., Engdahl, E. R., & Burdick, S., 2008. A new global model for P wave speed variations in Earth's mantle, Geochem. Geophys. Geosyst., 9.

Li, X. & Cormier, V. F., 2002. Frequency-dependent seismic attenuation in the inner core 1 . A viscoelastic interpretation, J. Geophys. Res., 107, 1-20.

Lincot, A., Merkel, S., & Cardin, P., 2015. Is inner core seismic anisotropy a marker for plastic flow of cubic iron?, Geophys. Res. Lett., pp. 1326–1333.

Lincot, A., Cardin, P., Deguen, R., & Merkel, S., 2016. Multiscale model of global inner-core anisotropy induced by hcp-alloy plasticity, Geophys. Res. Lett., pp. 1–23.

Lythgoe, K. H. & Deuss, A., 2015. The existence of radial anisotropy in Earth's upper inner core revealed from seismic normal mode observations, Geophys. Res. Lett., pp. 4841–4848.

Lythgoe, K. H., Deuss, A. F., Rudge, J. F., & Neufeld, J. A., 2014. Earths inner core: Innermost inner core or hemispherical variations? Earth and Planetary Science Letters, 385, 181–189.

Mikhaylushkin, A. S., Simak, S. I., Dubrovinsky, L., Dubrovinskaia, N., Johansson, B., & Abrikosov, I. A., 2007. Pure iron compressed and heated to extreme conditions, Phys. Rev. Lett., 99, 1–4.

Modak, P., Verma, A. K., Rao, R. S., Godwal, B. K., Stixrude, L., & Jeanloz, R., 2007. Stability of the hcp phase and temperature variation of the axial ratio of iron near Earth-core conditions, J. Phys. Condens. Matter, 19, 1–9.

Monnereau, M., Calvet, M., Margerin, L., & Souriau, A., 2010. Lopsided Growth of Earth's Inner Core, Science, 328, 1014–1017.

Morelli, A., Dziewonski, A. M., & Woodhouse, J. H., 1986. Anisotropy of the inner core inferred from PKIKP travel times, Geophys. Res. Lett., 13, 1545–1548.

Nguyen, J. H. & Holmes, N. C., 2004. Melting of iron at the physical conditions of the Earth's core, Nature, 720, 339–342.

Obayashi, M., Yoshimitsu, J., Nolet, G., Fukao, Y., Shiobara, H., Sugioka, H., Miyamachi, H., & Gao, Y., 2013. Finite frequency whole mantle P wave tomography: Improvement of subducted slab images, Geophys. Res. Lett., 40, 5652–5657.

Ritsema, J., Deuss, A. F., van Heijst, H. J., & Woodhouse, J. H., 2011. S40RTS: a degree-40 shear-velocity model for the mantle from new Rayleigh wave dispersion, teleseismic traveltime and normal-mode splitting function measurements, Geophys. J. Int., 184(3), 1223–1236.

Romanowicz, B., Tkalcic, H. & Breger, L., 2003. On the origin of complexity in PKP travel time data, in: Earth's Core: Dynamics, Structure, Rotation, Geodynamics Series 31, pp. 31–44, eds Dehant, V., et al American Geophysical Union, Washington, DC.

Romanowicz, B. & Wenk, H.-r., 2017. Anisotropy in the deep Earth, Phys. Earth planet. Int., 269, 58-90.

Rost, S. & Garnero, E. J., 2004. A study of the uppermost inner core from PKKP and PP differential traveltimes, Geophys. J. Int., 156, 565–574.

Rost, S., Garnero, E. J., & Williams, Q., 2006. Fine-scale ultralow-velocity zone structure from high-frequency seismic array data, Journal of Geophysical Research, 1-14.

Selby, N. D., 2008. Application of a Generalized F Detector at a Seismometer Array, Bull. seism. Soc. Am., 98, 2469–2481.

Sun, X. & Song, X., 2008. The inner inner core of the Earth : Texturing of iron crystals from three-dimensional seismic anisotropy, Earth Planet. Sci. Lett., 269, 56–65.

Tanaka, S. & Hamaguchi, H., 1997. Degree one heterogeneity and hemispherical variation of anisotropy in the inner core from PKP(BC)-PKP(DF) times, J. Geophys. Res., 102(96), 2925–2938.

Tateno, S., Hirose, K., Ohishi, Y., & Tatsumi, Y., 2010. The structure of iron in the Earth's Inner Core, Science, 330, 359–362.

Tkalcic, H., 2010. Large variations in travel times of mantle sensitive seismic waves from the South Sandwich Islands: Is the Earth's inner core a conglomerate of anisotropic domains?, Geophys. Res. Lett., 37, 1–6.

Tkalcic, H., 2015. Complex inner core of the Earth: The last frontier of global seismology, Reviews of Geophysics, pp. 59–94.

Waszek, L., Irving, J., & Deuss, A., 2011. Reconciling the hemispherical structure of Earth's inner core with its super-rotation, Nature Geosci., 4, 264–267.

Weber, M., 1990. Subduction zones - their influence ontravel times and amplitudes of of P-waves, Geophys. J. Int., 101, 529–544.

Weber, M. & Körnig, M., 1992. A search for anomalies in the lowermost mantle using seismic bulletins, Phys. Earth Planet. Int., 73, 1–28.

Wenk, H.-R., Baumgardner, J. R., Lebensohn, R. A., & Tome, C. N., 2000. A convection model to explain anisotropy of the inner core, J. Geophys. Res., 105, 5663{5677.

Woodhouse, J. H., Giardini, D., & Li, X.-d., 1986. Evidence for inner core anisotropy from free oscillations, Geophys. Res. Lett., 13(13), 1549–1552.